Inorganic Chemistry

Article

pubs.acs.org/IC

Synthesis and Photocatalytic Activity of Single-Crystalline Hollow rh-In_2O_3 Nanocrystals

Jiefu Yin and Huaqiang Cao*

Department of Chemistry, Tsinghua University, Beijing 100084, P. R. China

Supporting Information

ABSTRACT: We report here for the first time the hollow, metastable, single-crystal, rhombohedral In_2O_3 (rh-In_2O_3) nanocrystals synthesized by annealing solvothermally prepared InOOH solid nanocrystals under ambient pressure at 400 °C, through a mechanism of the Kirkendall effect, in which pore formation is attributed to the difference in diffusion rates of anions (OH^- and O^{2-}) in a diffusion couple. The InOOH solid nanocrystals were prepared via a controlled hydrolysis solvothermal route by using $In(NO_3)_3{\cdot}4.5H_2O$ as a starting material and glycerol–ethanol as a mixed solvent. The glycerol–ethanol mixed solvent plays a key role on the formation of the intermediate InOOH, thus the final product of rh-In_2O_3. The as-synthesized In_2O_3 nanocrystals present excellent photocatalytic degradation of rhodamine B (RhB) and methylene blue (MB) dyes, which present ~92% degradation of RhB or MB after 4 or 3 h reaction in the presence of the as-synthesized In_2O_3 nanocrystals, respectively.

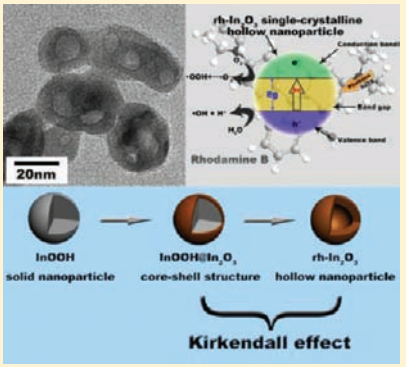

1. INTRODUCTION

Hollow nanocrystals[1] are important nanomaterials that exhibit many applications including using as catalysis,[2] solar cells,[3] magnetic resonance imaging (MRI),[4] drug delivery,[5] nano-electronics,[6] and nano-optics.[7] A general approach for synthesizing hollow nanocrystals is based on the sacrificial template methods—after the formation of shell structures coated on template agents, the templates are removed by thermal[8] or chemical etching treatments,[9] including acidic etching,[9a] redox etching,[9b] molten salt corrosion,[9c] and displacement reaction[1a,7] to generate the void space. Besides these methods, some processes have also been used to synthesize hollow nanocrystals such as a hydrothermal approach[10] and the nanoscale Kirkendall effect.[1b,11] Despite these, the challenge to control the synthesis of hollow single-crystal nanocrystals has been met with limited success. It is still a great challenge to synthesize hollow nanocrystals. We know that high-quality materials always yield new physicochemcial properties and applications. It is needed to exploit efficient controllable methods to generate hollow nanocrystals.

In_2O_3 is a polymorph, i.e., the stable cubic phase (body-centered cubic, bcc-In_2O_3) and the metastable rhombohedral phase (rhomb-centered hexagonal, denoted as rh-In_2O_3 hereafter).[12] Therein, rh-In_2O_3 is regarded as a high-pressure polymorphic substance of cubic In_2O_3, which is a metastable phase at atmospheric pressure.[13] In_2O_3, being an important semiconductor with a wide band gap (2.93 ± 0.15 eV for bcc-In_2O_3 and 3.02 ± 0.15 eV for rh-In_2O_3),[14] has been applied in lithium ion batteries,[15] solar cells,[16] computer touch screens,[17] sensors,[18] optoelectronic devices,[19] photocatalysis,[20] etc. However, most of the researches of In_2O_3 are focused on bcc-In_2O_3,[15−22] whereas the metastable rh-In_2O_3 has been seldom reported.[23] Li and co-workers reported bcc-In_2O_3 hollow microspheres via a surfactant-free vesicle-template-interface route.[20] Gurlo et al. synthesized hollow bcc-In_2O_3 microsphere and rh-In_2O_3 nanoparticles via a surfactant-free self-assembly route.[24] To the best of our knowledge, pure and hollow rh-In_2O_3 single-crystalline nanostructures have not been achieved under atmospheric pressure thus far, not to say nothing of the applications of rh-In_2O_3 in environmental applications.

Recently, it has aroused our great interest to prepare novel nanomaterials applying in photocatalytic degradation of organic dyes in wastewater, such as, SnO_2 nanocrsytals,[25] ZrO_2 nanocrystals,[26] $In(OH)_3$ nanocubes,[27] Ag_2Se complex nanostructures,[28] Bi@Bi_2O_3 microspheres,[29] and ZnSe microspheres.[30]

Herein, we report the synthesis of pure and hollow single-crystalline rh-In_2O_3 nanocrystals under mild synthesis conditions by annealing InOOH solid nanocrystal precursors at 400 °C at atmospheric pressure. The growth mechanism was demonstrated to abide by the nanoscale Kirkendall effect.[1b,11a,31] The novelty of the present study is related to the new synthesis strategy to generate pure metastable hollow rh-In_2O_3 nanocrystals by a simple solvothermal reaction followed by an annealing treatment process. The ethanol–glycerol mixed solvent used in the solvothermal reaction has been demonstrated to play a crucial role in the formation of hollow rh-In_2O_3 nanocrystals.

2. EXPERIMENTAL SECTION

2.1. Synthesis of rh-In_2O_3 Hollow Nanocrystals. $In(NO_3)_3{\cdot}4.5H_2O$ (Analytical pure, AR, Sinopharm Chemical Reagent

Received: January 2, 2012
Published: June 4, 2012

   dx.doi.org/10.1021/ic300005c | Inorg. Chem. 2012, 51, 6529−6536

Scheme 1. Possible Growth Mechanism of the As-Synthesized Hollow rh-In_2O_3 Nanocrystals

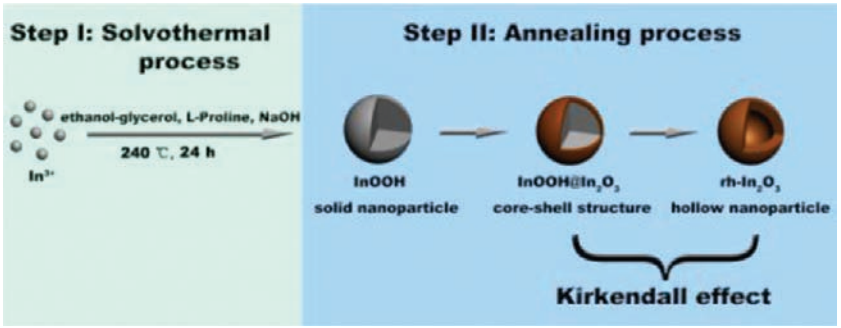

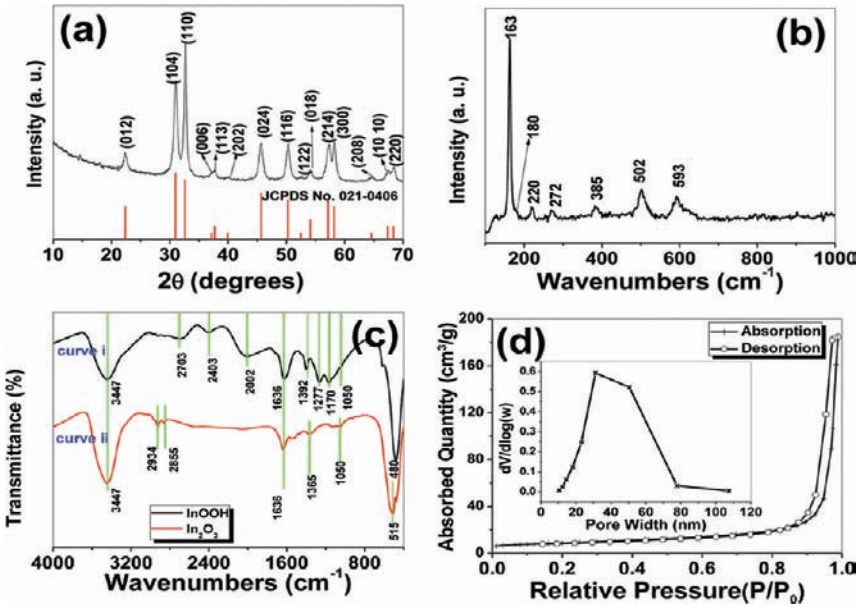

Figure 1. Characterization of as-synthesized In_2O_3: (a) XRD pattern, (b) Raman spectrum, (c) FT-IR spectrum, (d) nitrogen adsorption–desorption isothermals in nitrogen measured at 77 K, (inset) corresponding pore-size distribution.

Beijing Co, Ltd.) and L-proline ($C_5H_9NO_2$, >99%, Beijing Kebio Biotechnology Co., Ltd.) were used without further purification. In a typical synthesis, $In(NO_3)_3$ (1 mmol) and L-proline (8 mmol) were dissolved in 30 mL a mixed solvent of ethanol–glycerol (v:v = 2:1) with stirring until complete dissolution, leading to solution A. NaOH (0.64 g) was dissolved in 10 mL deionized water and formed solution B. Then, solution B was added dropwise into solution A with stirring for 30 min, followed by transferring into a Teflon-lined stainless steel autoclave. After the autoclave was heated at 240 °C for 24 h and cooled down to room temperature naturally, the products were collected and washed with ethanol for three times, followed by drying at 80 °C for 3 h. After annealing at 400 °C for 3 h in air under atmospheric pressure, the pure and hollow rh-In_2O_3 nanocrystals can be obtained.

2.2. Materials Characterization. The X-ray powder diffraction (XRD) measurement was carried out on a X-ray diffractometer (Druker D8 Advance) with Cu Kα radiation (λ = 1.54056 Å) in a 2θ range from 10° to 70°. Transmission electron microscopy (TEM) and high-resolution electron microscopy (HRTEM) measurement were carried out on a JEOL JEM-2010F electron microscope, operating at 120 kV. The UV–vis spectrum was monitored by using a UV–vis spectrometer (UNICO Corp. UV-2102PC). Fourier transform infrared (FT-IR) spectra were obtained on a Nicolet 560 FT-IR spectrophotometer. Raman spectra (Renishaw, RM 1000) were measured with excitation from the 514 nm line of Ar ion laser with a power of about 5 mW. Adsorption–desorption isotherms of nitrogen were recorded on BET Micromerities TriStar II 3020 equipment at 77 K. Thermal gravimetric analysis and differential thermal analysis (TGA/DTA) experiment was carried out on a TGA Q5000 V3.5 Build 252 in air atmosphere.

2.3. Photocatalytic Activity Test. The photocatalytic activity of the as-synthesized single-crystalline hollow rh-In_2O_3 nanocrystals was evaluated by photodegradation of rhodamine B (RhB) and methylene blue (MB) dye aqueous solutions under UV irradiation. A 250 W high-pressure mercury lamp (Beijing Huiyixin Electric Forces Technology Development Co., Ltd.) was set inside a cylindrical reactor and surrounded by a circulating water jacket to cool the lamp and minimize infrared radiation. An 80 mg portion of rh-In_2O_3 nanocrystals was suspended in 40 mL of aqueous solutions (RhB: 1 × 10^{-5} mol/L, MB: 2 × 10^{-5} mol/L). The solutions were continuously stirred for about 30 min at room temperature to ensure the estabishment of an adsorption–desorption equilibrium among the photocatalyst, RhB or MB, and water, before irradiation with UV light from the high-pressure mercury lamp. The distance between the light source and the bottom of the solution was about 10 cm. The concentration of RhB and MB was monitored by using a UV–vis spectrometer (Shimadzu UV-2100S spectrophotometer).

3. RESULTS AND ANALYSIS

The typical preparation procedure is shown in Scheme 1 (see the Experimental Section for details). An L-proline-assisted solvothermal route was selected as the first step. An NaOH solution was added dropwise into a solution containing $In(NO_3)_3$, L-proline, and ethanol–glycerol mixed solvent with stirring for 30 min, followed by solvothermal treatment at 240

dx.doi.org/10.1021/ic300005c | Inorg. Chem. 2012, 51, 6529–6536

°C for 24 h, cool down to room temperature naturally, as well as washing and drying at 80 °C for 3 h, in succession. After annealing treatment at 400 °C for 3 h in air under atmospheric pressure, pure and hollow rh-In_2O_3 nanocrystals were obtained with the yield of ~97%.

3.1. Characterization of As-Synthesized Samples. The XRD pattern of the as-synthesized sample is shows in Figure 1a. The diffraction peaks are consistent with those of rh-In_2O_3 (JCPDS no: 021-0406). No impurity peaks can be detected, suggesting the final product to be pure phase of rh-In_2O_3. The XRD pattern of the precursor before an annealing treatment process shows that it belongs to orthorhombic InOOH (Supporting Information Figure S1, JCPDS no: 017-0549). It is known that the diffraction peak at $2\theta = 32.7°$ [(110)] is the characteristic peak of rhombohedral phase of In_2O_3, while the diffraction peak at $2\theta = 30.62°$ [(222)] is the characteristic peak of cubic phase of In_2O_3.[32] The averaged size of In_2O_3 is ca. 15.1 nm based on the Scherrer formula (Supporting Information, SI, Table S1).

The In_2O_3 phase was further characterized by its Raman spectrum (Figure 1b). According to the crystallography data, the rh-In_2O_3 crystal structure belongs to space group $R\bar{3}c$, with the point group $D^6 3d$. On the basis of the group theory analysis, the optical modes have the irreducible representation, shown as below:[33]

$$\Gamma_{opt} = 2A_{1g} + 5E_g + 2A_{1u} + 2A_{2u} + 3A_{2g} + 4E_u \quad (1)$$

The A_{1g} and E_g are Raman active, while the A_{1u}, A_{2u}, A_{2g}, and E_u are infrared active or Raman inactive. The Raman modes centered at 163, 180, 220, 272, 385, 502, and 593 cm^{-1} can be observed. The Raman modes at 163 and 502 cm^{-1} are attributed to the A_{1g} mode, while the Raman modes at 180, 220, 272, 385, and 593 cm^{-1} are assigned to the E_g mode, which agree well with the reported values in the literature.[34] Most importantly, the Raman data further demonstrate that the hollow In_2O_3 nanocrystals are indeed single crystalline structure of rh-In_2O_3.[23c,34]

Figure 1c showed the Fourier transform infrared (FT-IR) spectra of the intermediate InOOH (curve i) and final product rh-In_2O_3 (curve ii). In curve i, the broad peak centered at 3447 cm^{-1}, accompanying by a weak peak at 1636 cm^{-1}, is attributed to the O−H stretching vibration (ν_{O-H}) from residual water in KBr discs,[35] which also appears at curve ii, i.e., the FT-IR spectrum of In_2O_3. The peaks at 2703 and 2002 cm^{-1} are typical O−H stretching vibrations (ν_{O-H}) of InOOH. However, these peaks disappear in curve ii, suggesting that the transformation from InOOH to In_2O_3 is complete.[36] The peaks at 1050, 1170, 1277, and 1392 cm^{-1} are attributed to typical O−H bending, or deformation vibration (δ_{O-H}).[33,35] The peak at 480 cm^{-1} is attributed to the In−O vibration.[37] The peak at 2403 cm^{-1} can be attributed to the absorption peak of adsorbed CO_2,[38] coming from the heat decompose of organic solvents and L-proline. However, in the curve ii, the peak at 3447 cm^{-1}, accompanying by a weak peak at 1636 cm^{-1}, is due to the O−H stretching vibration (ν_{O-H}) from residual water in KBr discs for FT-IR measurement.[35] The peaks at 1050 and 1365 cm^{-1} are attributed to typical O−H bending vibration (δ_{O-H}).[33] The peak at 515 cm^{-1} is attributed to In−O vibration.[36] The O−H absorption peaks at 2703 and 2002 cm^{-1} of InOOH after annealing treatment disappear in In_2O_3. This phenomenon further demonstrates that the transformation of InOOH to In_2O_3 is complete. The peaks at 2855 and 2934 cm^{-1} may be attributed to $\nu_s(CH_2)$ and $\nu_{as}(CH_2)$, respectively,[35] coming from the heat decompose of organic solvents and L-proline.

N_2 adsorption−desorption analysis of the as-synthesized In_2O_3 revealed a typical type-IV isotherm with an evident hysteresis loop in the range of $0.87 < P/P_0 < 1.0$ (Figure 1d). The characteristic hysteresis loop of the type-IV isotherm is indicative of small mesopores (i.e., 2−50 nm in pore sizes).[39] Brunauer−Emmett−Teller (BET) measurement shows that the as-synthesized In_2O_3 nanocrystals have a specific surface area of about 30.73 m^2/g. Pore size calculated from adsorption branch of the N_2 isotherm is ~31.2 nm, agreeing with HRTEM observation with a little error.

The morphology and microstructure of the as-synthesized In_2O_3 sample was further examined by TEM and HRTEM observation. Figure 2a−c shows TEM and HRTEM images of

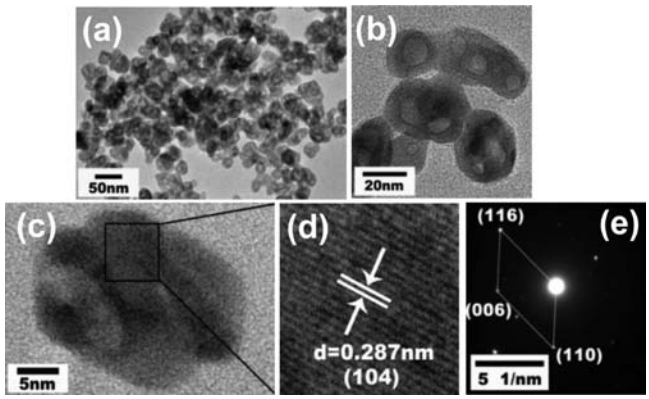

Figure 2. (a and b) TEM images, (c and d) HRTEM images, and (e) SAED pattern of rh-In_2O_3.

rh-In_2O_3 hollow nanocrystals; they have pale regions in the center in contrast to dark edges, indicating they are hollow spheres with 10−30 nm in overall diameter and 10 nm in inner diameter of holes (Figure 2a and b). The high-quality single-crystalline nature of the as-synthesized hollow rh-In_2O_3 spheres is also confirmed by the HRTEM analysis and selected area of electron diffraction (SAED) (Figure 2c−e). The HRTEM images present well-defined lattice fringes with an interplanar distance of 0.287 nm, corresponding to the {104} interplanar distance of rh-In_2O_3, which demonstrates the hollow feature of the spheres.

To study the void evolution process from orthorhombic InOOH solid nanocrystals to rh-In_2O_3 hollow nanocrystals during the annealing process, we took a TGA/DTA experiment for the as-synthesized intermediate InOOH in air atmosphere, as shown in Figure 3. The TGA curve can be mainly divided into two weight-loss steps. The first step was taken place between ~25 and ~240 °C, which can be attributed to a great of physical water evaporation from the surface of InOOH. The weight loss of this step was ~2%, and at the same time the DTA curve shows a negative temperature differential, suggesting an endothermic reaction. The second step of the TGA curve was occurred between ~240 and ~800 °C, suggesting an endothermic decomposition reaction process, $2InOOH \rightarrow$ rh-$In_2O_3 + H_2O\uparrow$. The weight loss of this step was ~11.2%, consistent with the theoretical analysis (12.2%) within the error. On the basis of the TGA curve observation, we find that the metastable rh-In_2O_3 is close to completely changing from InOOH after annealing the InOOH at 400 °C under ambient pressure.

dx.doi.org/10.1021/ic300005c | Inorg. Chem. 2012, 51, 6529−6536

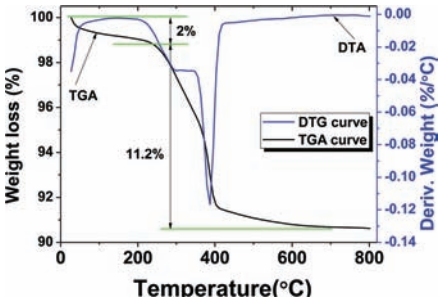

Figure 3. TGA and DTA curves of the InOOH powder tested in air at a temperature raising rate of 10 °C/min.

The structure evolution process from orthorhombic InOOH to rh-In_2O_3 nanoctystals can be further detected by the XRD (Figure 4). It demonstrates that the phase transformation starts

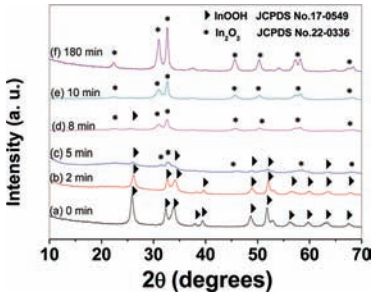

Figure 4. XRD patterns of the structure evolution by annealing InOOH nanocrystals at 400 °C under ambient pressure with different annealing time: (a) 0, (b) 2, (c) 5, (d) 8, (e) 10, and (f) 180 min.

after annealing for 5 min, while the transformation is finished at 10 min. The strong and sharp diffraction peaks of InOOH (curve a in Figure 4) and rh-In_2O_3 (curve f in Figure 4) indicate that both InOOH and rh-In_2O_3 are well crystallized, which can be further demonstrated by corresponding HRTEM observation (Figure 5).

3.2. Growth Mechanism of As-Synthesized rh-In_2O_3 Hollow Nanocrystals. The possible formation mechanism of rh-In_2O_3 hollow nanocrystals is divided into two processes, i.e., the formation of InOOH solid nanocrystals generated in the solvothermal reaction (Figure 5a) and the complete formation of rh-In_2O_3 hollow nanocrystals after an annealing process (Figure 5c–e).

In the first stage, the InOOH solid nanocrystals were formed by a hydrolysis reaction of In^{3+} under a solvothermal condition in the temperature range of 180–240 °C. We found the glycerol (boiling point: 290 °C) and ethanol mixed solvent was responsible for the formation of InOOH solid spheres, while cubic $In(OH)_3$ was generated by using other solvents, such as glycol (boiling point: 197.3 °C) and ethanol mixed solvent, PEG (polyethylene glycol, M = 400; boiling point: 250 °C) and ethanol mixed solvent, and ethanol (boiling point: 78.3 °C), under the same solvothermal condition (eqs 2 or 3) (Figure 6 and 7). The detailed chemical reactions are suggested as follows:

$$In^{3+} + 3OH^{-}(\text{in glycerol–ethanol solvent}) \rightarrow InOOH + 2H_2O \quad (2)$$

or

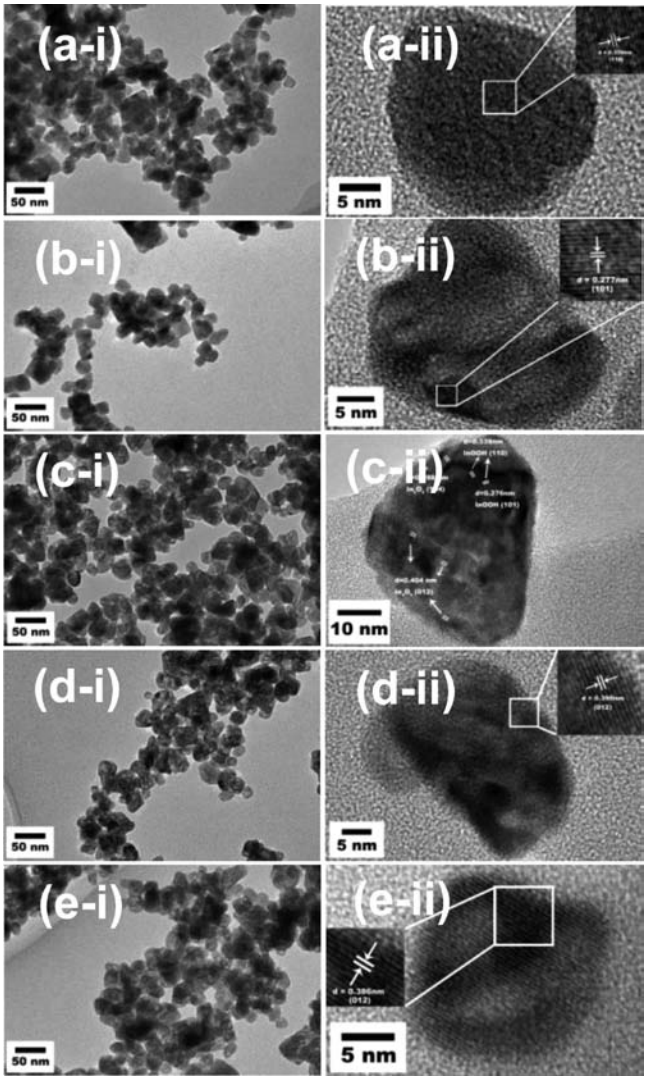

Figure 5. TEM (i) and HRTEM (ii) images of the structure evolution by annealing InOOH nanocrystals at 400 °C under ambient pressure with different annealing time: (a) 0, (b) 2, (c) 5, (d) 8, and (e) 10 min.

$$In^{3+} + 3OH^{-}(\text{in other solvents}) \rightarrow In(OH)_3 \quad (3)$$

Bcc-In_2O_3 can be obtained after annealing the intermediate precursor $In(OH)_3$ ($2In(OH)_3 \rightarrow$ bcc-$In_2O_3 + 3H_2O$), while rh-In_2O_3 can be obtained after annealing InOOH ($2InOOH \rightarrow$ rh-$In_2O_3 + H_2O\uparrow$) (Figure 7 and SI Figure S2). Obviously, the glycerol–ethanol mixed solvent plays a key role for the

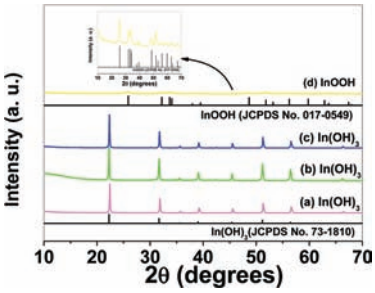

Figure 6. XRD patterns of the intermediate samples synthesized in the solvothermal reaction with different solvents (a) ethanol–glycol, (b) ethanol, (c) ethanol–PEG, and (d) ethanol–glycerol.

dx.doi.org/10.1021/ic300005c | Inorg. Chem. 2012, 51, 6529–6536

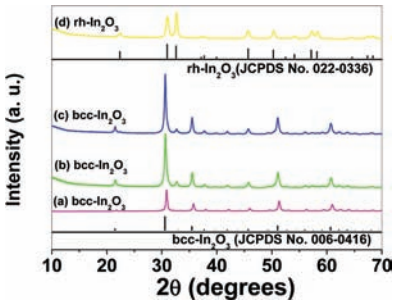

Figure 7. XRD patterns of the final samples synthesized by annealing the precursors which were synthesized in the solvothermal reaction with different solvents composed of (a) ethanol–glycol, (b) ethanol, (c) ethanol–PEG, and (d) ethanol–glycerol.

formation of the InOOH, thus the formation of rh-In_2O_3. The boiling point of glycerol is the highest among these used solvents. Under the solvothermal conditions, glycerol will keep in liquid state, while others are in gas state. The liquid glycerol may form hydrogen bonds with InOOH which may favor the stabilization of InOOH. The detailed process needs further investigated.

In the second stage, the solid InOOH was transferred into hollow rh-In_2O_3. The Kirkendall effect leads to Kirkendall porosity though the supersaturation of vacancies into hollow pores.[40] The decomposition of surface InOOH occurred and, thus, generated an In_2O_3 layer coated on the InOOH core after an annealing process in 5 min. This process has been demonstrated by the XRD data (Figure 4). Here the anion exchange occurred between OH^- of InOOH with O^{2-} of In_2O_3 in a nanoscale InOOH@In_2O_3 structure system, leading to hollow structures rather than solid nanoparticles.

It is worth pointing out that the final product is a single-crystalline hollow structure of rh-In_2O_3. It is known that single-crystalline hollow structures are rarely obtained.[11a,41] Usually, poorly bonded atoms diffuse more rapidly than those which are similar in size and valence.[42] The In–OH bond in InOOH is weaker than the In–O bond in In_2O_3, based on the thermal stability of InOOH and In_2O_3.[43] So, the diffusion rate of OH^- (radii of OH^- = 137 pm) is larger than that of O^{2-} (radii of O^{2-} = 140 pm).[44] The anion in oxides usually has the smallest diffusion coefficient because it is usually larger than the cations.[42] Diffusion is a basic process involved in crystals. An ion can diffuse by moving into an adjacent vacancy of the same kind.[45] Inward ion diffusion is limited, but core species diffusion outward is forceful, which is favorable to the formation of a void space inside the nanocrystals. That means the faster diffusion of outward OH^- than incoming O^{2-} leads to the formation of a hollow structure and H_2O vapor is released from the nanocrystals. Once the In_2O_3 shell is generated after annealing InOOH, outward OH^- diffusion will spontaneously proceed without the help of further anion exchange for releasing the interface energy in the InOOH@In_2O_3 structure, fully converting into In_2O_3 hollow nanocrystals. To the best of our knowledge, this is the second report of Kirkendall effect in anion exchange.[11a] HRTEM images demonstrated the complete conversion from the initial solid InOOH nanoparticles into In_2O_3 hollow nanocrystals (Figure 5ii).

3.3. Photocatalytic Activity of As-Synthesized rh-In_2O_3 Hollow Nanocrystals. The photocatalytic activities of the as-synthesized single-crystalline hollow rh-In_2O_3 nanocrystals were evaluated using degradation of RhB (1×10^{-5} mol/L) and MB (2×10^{-5} mol/L) dyes in aqueous solutions under UV light irradiation at room temperature, respectively.

The characteristic absorption peak of RhB at λ = 553 nm was selected as monitoring the photocatalytic degradation process of RhB. In the absence of rh-In_2O_3 nanocrystals under UV light, the photodegradation of RhB was negligible (SI Figure S3a). The photodegradation in the presence of rh-In_2O_3 nanocrystals in darkness was only about 13.7% after 8 h (SI Figure S3b). In comparison, the photolytic degradation of RhB in aqueous solution under UV irradiation in the presence of commercial In_2O_3 (Tianjin Guangfu Research Institute) was also carried out under the same condition. Figure 8a and 8b show the

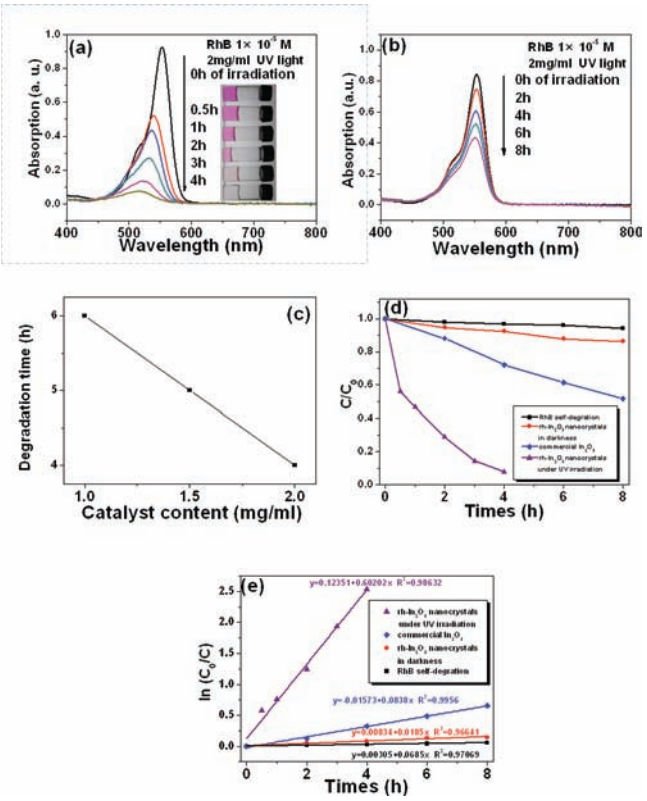

Figure 8. (a) Temporal UV–vis absorption spectral changes and corresponding color changes (inset) of RhB in water in the presence of as-synthesized, single-crystalline, hollow rh-In_2O_3 nanocrystals under UV irradiation. (b) Temporal UV–vis absorption spectral changes of RhB in water in the presence of commercial In_2O_3. (c) Relationship between rh-In_2O_3 nanocrystals catalyst content and degradation time. (d) Photodegradation curves of RhB as a function of irradiation time. (e) Corresponding selected fitting results using pseudo-first-order reaction kinetics.

photodegradation of RhB in the presence of rh-In_2O_3 nanocrystals (content: 80 mg of rh-In_2O_3 nanocrystals with the content of 2 mg/mL) and commercial In_2O_3, respectively. The absorption maxima of the treated solution in the presence of rh-In_2O_3 nanocrystals at various times exhibited hypsochromic shifts. After 4 h irradiation under UV light, the photodegradation of RhB dye solution with rh-In_2O_3 nanocrystals was ~92%, close to 100%, accompanied by the color changing from violet red to colorless. However, if we decrease the catalyst content from 2 to 1.5 or 1 mg/mL, the degradation times increase from 4 to 5 or 6 h with the degradation ratio reaching ~92%, respectively (SI Figure S4a and 4b). It exhibits inverse dependent relationship between catalyst content and

dx.doi.org/10.1021/ic300005c | Inorg. Chem. 2012, 51, 6529–6536

degradation time (Figure 8c). Nevertheless, the photodegradation in the presence of commercial In_2O_3 was only 48.2% after 8 h (Figure 8b). This is attributed to the large surface-to-volume ratio and the high-quality single-crystalline nature of rh-In_2O_3 nanocrystals, which is favorable to increasing the photocatalytic reaction sites.[46] These results suggest that the as-synthesized rh-In_2O_3 nanocrystals indeed possess intrinsic photocatalytic activity under UV light irradiation. Figure 8d shows the photodegradation efficiencies of RhB in different conditions. The linear relationship between ln c_0/c and t is shown in Figure 8e, confirming that the photodegradation reaction is indeed pseudo-first-order that can be fitted to the equation:

$$\ln c_0/c = kt \quad (4)$$

where c_0 and c indicate the initial RhB concentration and that after irradiation time t, and k is the reaction rate constant, respectively.[47] The pseudo-first-order rate constants for the degradation of RhB are 0.6020 and 0.0838 h^{-1} in the presence of rh-In_2O_3 nanocrystals and commercial In_2O_3, respectively, while the pseudo-first-order rate constants for the degradation of RhB at the presence of rh-In_2O_3 nanocrystals in darkness or in the absence of catalyst are only 0.0185 or 0.0068 h^{-1}, respectively.

To further investigate the photocatalytic activity of rh-In_2O_3 nanocrystals, we study the photodegradation of MB molecule in aqueous solution under UV light irradiation at room temperature. The characteristic absorption peak of MB at λ = 664 nm was selected as monitoring the photocatalytic degradation process of MB. Figure 9a shows the photodegradation of MB in the presence of rh-In_2O_3 nanocrystals (content: 80 mg of rh-In_2O_3 nanocrystals with the content of 2 mg/mL), the photodegradation of MB dye solution was about 92% after 3 h irradiation under UV light; however, after 8 h irradiation, the photodegradation of MB was only 42% at the presence of commercial In_2O_3 with other parameters unchanged (Figure 9b). However, if we decrease the catalyst content from 2 to 1.5 or 1 mg/mL, the degradation times increase from 3 to 6 or 10 h with the degradation ratio reaching ~92%, respectively (SI Figure S6a and S6b). It also exhibits inverse dependent relationship between catalyst content and degradation time (Figure 9c). The photodegradation efficiencies of MB in different conditions were shown in Figure 9d, there was only 19.2% degradation of MB dye solution after 8 h irradiation under UV light without rh-In_2O_3 nanocrystals, and 43.4% degradation after 8 h irradiation at the presence of rh-In_2O_3 nanocrystals in darkness. Figure 9e shows the linear relationship between ln c_0/c and t, the corresponding pseudo-first-order rate constants for the degradation of MB dye solution with rh-In_2O_3 nanocrystals, commercial In_2O_3 were 0.8347 and 0.0699 h^{-1} respectively, while the constant was only 0.0656 h^{-1} with the presence of rh-In_2O_3 nanocrystals in darkness, and only 0.0272 h^{-1} without catalyst. These results demonstrated that the as-synthesized single-crystalline hollow rh-In_2O_3 nanocrystals have high photocatalytic activity which can be utilized in the removal of dye molecules in aqueous solution.

The degradation mechanism of the RhB over In_2O_3 nanocrystals under UV light is shown in Figure 10, termed as photodegradation, which can creat free radicals. Once this reaction starts, it sets off a chain reaction that accelerates degradation unless stabilizers are used to interrupt the oxidation cycle.[48]

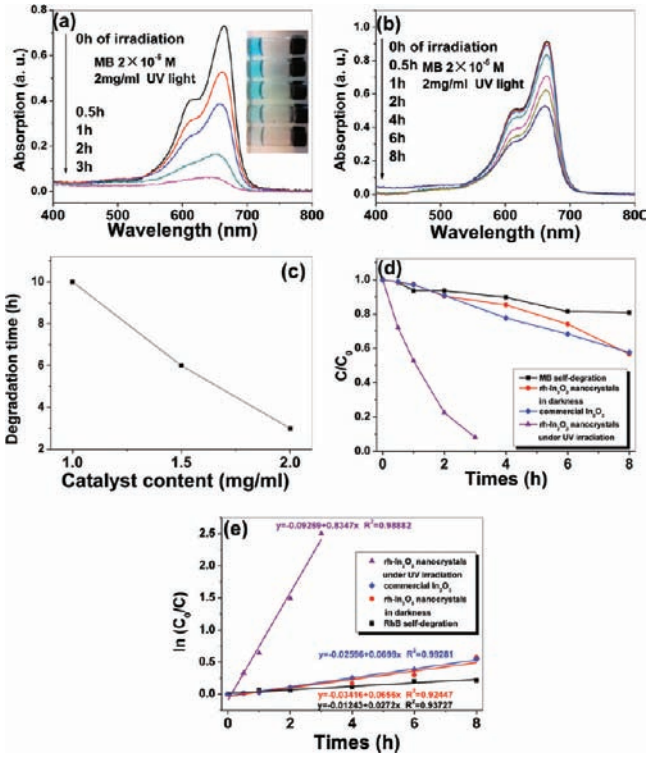

Figure 9. (a) Temporal UV−vis absorption spectral changes and corresponding color changes (inset) of MB in water in the presence of the as-synthesized single-crystalline hollow rh-In_2O_3 nanocrystals under UV irradiation. (b) Temporal UV−vis absorption spectral changes of MB in water in the presence of commercial In_2O_3. (c) Relationship between rh-In_2O_3 nanocrystals catalyst content and degradation time. (d) Photodegradation curves of MB as a function of irradiation time. (e) Corresponding selected fitting results using pseudo-first-order reaction kinetics.

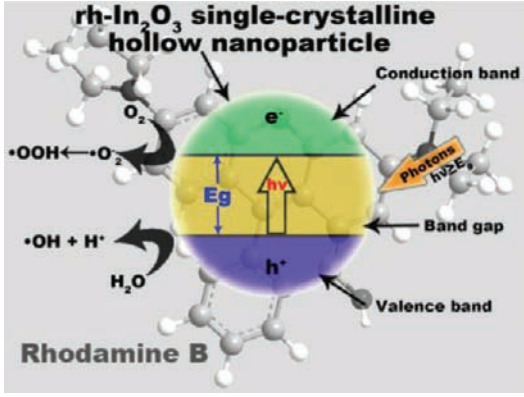

Figure 10. Degradation mechanism of dye molecules in aqueous solution (taking RhB, as an example).

It is well-known that In_2O_3 is an important n-type semiconductor. The as-synthesized single-crystalline hollow rh-In_2O_3 nanocrystals present a UV absorption maxima around 314 nm (3.95 eV in photon energy), which is blue-shifted in comparison with the band gap at 337 nm (3.67 eV in photon energy) of the bulk In_2O_3.[49] This blue shift is attributed to the existence of a weak quantum confinement effect (SI Figure S7).[50] When absorbing UV light with an energy of $h\nu$ matches or exceeds the band gap energy, E_g, the rh-In_2O_3 nanocrystals

dx.doi.org/10.1021/ic300005c | Inorg. Chem. 2012, 51, 6529−6536

generate valence-band holes (h^+) and conduction-band electrons (e^-) pairs at the surface, which is shown in eqs 5:

$$2In_2O_3 + h\nu \rightarrow In_2O_3(h^+) + In_2O_3(e^-) \quad (5)$$

And the holes can react with water adsorbed on the surface of rh-In_2O_3 nanocrystals to generate highly reactive hydroxyl radicals (·OH), at the same time O_2 acts as an electron acceptor to generate a superoxide anion radical ($\cdot O_2^-$), which combines with protons to generate ·OOH, as shown in eqs 6−8:[25,28,30,51]

$$H_2O + In_2O_3(h^+) \rightarrow \cdot OH + H^+ + In_2O_3 \quad (6)$$

$$O_2 + In_2O_3(e^-) \rightarrow \cdot O_2^{--} + In_2O_3 \quad (7)$$

$$O_2 + H^+ \rightarrow \cdot OOH \quad (8)$$

The ·OH radical is a rather reactive species that degrades many classes of organic substrates.[52] It is regarded that oxidative degradation of RhB and MB is generally caused by the subsequent attacks of $\cdot O_2^-$, ·OH, and ·OOH radicals through reaction 9 and reaction 10.[52,53]

$$\text{RhB} + O_2/O_2^-/\cdot OOH \rightarrow (\text{intermediates}) \rightarrow \text{degrade products} \quad (9)$$

$$\text{MB} + O_2/O_2^-/\cdot OOH \rightarrow (\text{intermediates}) \rightarrow \text{degrade products} \quad (10)$$

In comparison, hierarchical ZnO hollow spheroids (content: 0.5 mg/mL) exhibited the photocatalytic ability for RhB (1×10^{-5} M) under UV irradiation of lower than 60% in 5 h (or 300 min),[54] while our rh-In_2O_3 nanocrystals exhibited the photocatalytic ability for RhB (1×10^{-5} M) under UV irradiation of 92% in 4−6 h with the catalyst content ranging from 2 to 1 mg/mL. The photocatalytic ability for RhB (1×10^{-5} M) in the presence of mixed-phase TiO_2 nanocrystals (content: 1 mg/mL) under artificial solar light irradiation showed the degradation pseudo-first-order rate constants of 0.3531 (T1 sample), 0.1260 (T2 sample), 0.1299 (T4 sample), 0.1252 (T5 sample), and 0.1504 h^{-1} (P25 sample) lower than the constant of our rh-In_2O_3 nanocrystals (0.6020 h^{-1}) except the constant of 0.8971 h^{-1} for T3.[55] TiO_2 coated alumina membrane exhibited photocatalytic ability for MB (0.01 mM, i.e., 1×10^{-5} M) under UV illumination of close to 90% after 20 h,[56] while our rh-In_2O_3 nanocrystals showed the degradation times ranging from 3 to 6 or 10 h with the degradation ratio of MB reaching ~92% with the catalyst content ranging from 2 to 1.5 or 1 mg/mL, respectively.

4. CONCLUSIONS

In summary, single-crystalline, hollow, metastable rh-In_2O_3 nanocrystals were synthesized via abiding by a mechanism of the Kirkendall effect. The rh-In_2O_3 nanocrystals exhibit excellent photocatalytic activities for degenerating RhB and MB under UV irradiation, reaching at ~92% degradation after 4 or 3 h UV irradiation, respectively. These results can be attributed to the more oxygen vacancies on the surface of the In_2O_3 nanocrystals. The degradation rates of rh-In_2O_3 nanocrystals are 7.2 times or 11.9 times those of commercial In_2O_3 powder for RhB and MB degradation, respectively, suggesting that the as-synthesized In_2O_3 nanocrystals are a more powerful photocatalyst for the degradation of RhB and MB dyes.

■ ASSOCIATED CONTENT

Supporting Information

XRD pattern of intermideate product InOOH, TEM images of the samples synthesized with different solvents: (a) ethanol−glycol, (b) ethanol, (c) ethanol−PEG, (d) ethanol−glycerol. Temporal UV−vis absorption spectral changes of RhB and MB. UV−vis spectrum of the as-synthesized single-crystalline hollow rh-In_2O_3 nanocrystals. This material is available free of charge via the Internet at http://pubs.acs.org.

■ AUTHOR INFORMATION

Corresponding Author

*E-mail: hqcao@mail.tsinghua.edu.cn.

Notes

The authors declare no competing financial interest.

■ ACKNOWLEDGMENTS

Financial support from the National Natural Science Foundation of China (No. 20921001) is acknowledged.

■ REFERENCES

(1) (a) Sun, Y.; Xia, Y. *Science* **2002**, *298*, 2176. (b) Yin, Y.; Rioux, R. M.; Erdonmez, C. K.; Hughes, S.; Somorjai, G. A.; Alivisatos, A. P. *Science* **2004**, *304*, 711.
(2) Dhas, N. A.; Suslick, K. S. *J. Am. Chem. Soc.* **2005**, *127*, 2368.
(3) Hung, L.-I.; Tsung, C.-K.; Huang, W.; Yang, P. *Adv. Mater.* **2010**, *22*, 1910.
(4) Kim, T.; Momin, E.; Choi, J.; Yuan, K.; Zaidi, H.; Kim, J.; Park, M.; Lee, N.; McMahon, M. T.; Quinones-Hinojosa, A.; Bulte, J. W. M.; Hyeon, T.; Gilad, A. A. *J. Am. Chem. Soc.* **2011**, *133*, 2955.
(5) Shin, J.; Anisur, R. M.; Ko, M. K.; Im, G. H.; Lee, J. H.; Lee, I. S. *Angew. Chem., Int. Ed.* **2009**, *48*, 321.
(6) Zhang, W. F.; He, Z. B.; Yuan, G. D.; Jie, J. S.; Luo, L. B.; Zhang, X. J.; Chen, Z. H.; Lee, C. S.; Zhang, W. J.; Lee, S. T. *Appl. Phys. Lett.* **2009**, *94*, 123103.
(7) Zeng, J.; Huang, J.; Lu, W.; Wang, X.; Wang, B.; Zhang, S.; Hou, J. *Adv. Mater.* **2007**, *19*, 2172.
(8) Bang, J. H.; Suslick, K. S. *J. Am. Chem. Soc.* **2007**, *129*, 2242.
(9) (a) Kuo, C.-H.; Huang, M. H. *J. Am. Chem. Soc.* **2008**, *130*, 12815. (b) Wang, Z.; Luan, D.; Li, C. M.; Su, F.; Madhavi, S.; Boey, F. Y. C.; Lou, X. W. *J. Am. Chem. Soc.* **2010**, *132*, 16271. (c) Kim, D.; Park, J.; An, K.; Yang, N.-K.; Park, J.-G.; Hyeon, T. *J. Am. Chem. Soc.* **2007**, *129*, 5812.
(10) Huang, X.; Zhang, H.; Guo, C.; Zhou, Z.; Zheng, N. *Angew. Chem., Int. Ed.* **2009**, *48*, 4808.
(11) (a) Park, J.; Zheng, H.; Jun, Y.-W.; Alivisatos, A. P. *J. Am. Chem. Soc.* **2009**, *131*, 13943. (b) Peng, S.; Sun, S. *Angew. Chem., Int. Ed.* **2007**, *46*, 4155.
(12) Farvid, S. S.; Wang, T.; Radovanovic, P. V. *J. Am. Chem. Soc.* **2011**, *133*, 6711.
(13) Park, Y.-G.; Seo, K.-H.; Lee, J.-H.; Kim, J.-J.; Cho, S.-H.; O'Conner, C. J.; Lee, J.-S. *J. Electroceram.* **2004**, *13*, 851.
(14) King, P. D. C.; Veal, T. D.; Fuchs, F.; Ch. Wang, Y.; Payne, D. J.; Bourlange, A.; Zhang, H.; G. Bell, R.; Cimalla, V.; Ambacher, O.; Egdell, R. G.; Bechstedt, F.; McConvile, C. F. *Phys. Rev. B* **2009**, *79*, 205211.
(15) Kim, D.-W.; Hwang, I.-S.; Kwon, S. J.; Kang, H.-Y.; Park, K.-S.; Choi, Y.-J.; Choi, K.-J.; Park, J.-G. *Nano Lett.* **2007**, *7*, 3041.
(16) Park, K.-S.; Choi, Y.-J.; Kang, J.-G.; Sung, Y.-M.; Park, J.-G. *Nanotechnology* **2011**, *22*, 285712.
(17) Parthiban, S.; Ramamurthi, K.; Elangovan, E.; Martins, R.; Fortunato, E. *Appl. Phys. Lett.* **2009**, *94*, 212101.

(18) Du, N.; Zhang, H.; Chen, B.; Ma, X.; Liu, Z.; Wu, J.; Yang, D. *Adv. Mater.* **2007**, *19*, 1641.
(19) Cao, H.; Qiu, X.; Liang, Y.; Zhu, Q.; Zhao, M. *Appl. Phys. Lett.* **2003**, *83*, 761.
(20) Li, B.; Xie, Y.; Jing, M.; Rong, G.; Tang, Y.; Zhang, G. *Langmuir* **2006**, *22*, 9380.
(21) Chang, J.; Lee, W.; Mane, R. S.; Cho, B. W.; Han, S.-H. *Electrochem. Solid State* **2008**, *11*, A9.
(22) (a) Pinna, N.; Neri, G.; Antonietti, M.; Niederberger, M. *Angew. Chem., Int. Ed.* **2004**, *43*, 4345. (b) Lao, J.; Huang, J.; Wang, D.; Ren, Z. *Adv. Mater.* **2004**, *16*, 65. (c) Yang, H.; Shi, Q.; Tian, B.; Lu, Q.; Gao, F.; Xie, S.; Fan, J.; Yu, C.; Tu, B.; Zhao, D. *J. Am. Chem. Soc.* **2003**, *125*, 4724. (d) Tian, B.; Liu, X.; Solovyov, L. A.; Liu, Z.; Yang, H.; Zhang, Z.; Xie, S.; Zhang, F.; Tu, B.; Yu, C.; Terasaki, O.; Zhao, D. *J. Am. Chem. Soc.* **2004**, *126*, 865. (e) Lu, W.; Liu, Q.; Sun, Z.; He, J.; Ezeolu, C.; Fang, J. *J. Am. Chem. Soc.* **2008**, *130*, 6983. (f) Kim, H. S.; Byrne, P. D.; Facchetti, A.; Marks, T. J. *J. Am. Chem. Soc.* **2008**, *130*, 12580.
(23) (a) Epifani, M.; Siciliano, P. *J. Am. Chem. Soc.* **2004**, *126*, 4078. (b) Lee, C. H.; Kim, M.; Kim, T.; Kim, A.; Paek, J.; Lee, J. W.; Choi, S.-Y.; Kim, K.; Park, J.-B.; Lee, K. *J. Am. Chem. Soc.* **2006**, *128*, 9326. (c) Yu, D.; Yu, S.-H.; Zhang, S.; Zuo, J.; Wang, D.; Qian, Y. *Adv. Funct. Mater.* **2003**, *13*, 497.
(24) Gurlo, A.; Miehe, G.; Riedel, R. *Chem. Commun.* **2009**, 2747–2749.
(25) Wu, S.; Cao, H.; Yin, S.; Liu, X.; Zhang, X. *J. Phys. Chem. C* **2009**, *113*, 17893.
(26) Zheng, H.; Liu, K.; Cao, H.; Zhang, X. *J. Phys. Chem. C* **2009**, *113*, 18259.
(27) Cao, H.; Zheng, H.; Liu, K.; Fu, R. *Cryst. Growth Des.* **2010**, *10*, 597.
(28) Cao, H.; Xiao, Y.; Lu, Y.; Yin, J.; Li, B.; Wu, S.; Wu, X. *Nano Res.* **2010**, *3*, 863.
(29) Liu, X.; Cao, H.; Yin, J. *Nano Res.* **2011**, *4*, 470.
(30) Cao, H.; Xiao, Y.; Zhang, S. *Nanotechnology* **2011**, *22*, 015604.
(31) (a) Fan, H. J.; Knez, M.; Scholz, R.; Nielsch, K.; Pippel, E.; Hesse, D.; Zacharias, M.; Gösele, U. *Nat. Mater.* **2006**, *5*, 627. (b) Gao, J.; Zhang, B.; Zhang, X.; Xu, B. *Angew. Chem., Int. Ed.* **2006**, *45*, 1220. (c) Gao, J.; Liang, G.; Zhang, B.; Kuang, Y.; Zhang, X.; Xu, B. *J. Am. Chem. Soc.* **2007**, *129*, 1428.
(32) Kadir, A.; Mukhopadhyay, S.; Ganguli, T.; Galande, C.; Gokhale, M. R.; Arora, B. M.; Raychaudhuri, P.; Bhattacharya, A. *Solid State Commun.* **2008**, *149*, 361.
(33) Hollas, J. M. *Modern Spectroscopy*, 4th ed.; John Wiley & Sons Ltd.: West Sussex, England, 2004.
(34) Dong, H.; Chen, Z.; Sun, L.; Zhou, L.; Ling, Y.; Yu, C.; Tan, H. H.; Jagadish, Shen, C.; X.. *J. Phys. Chem. C* **2009**, *113*, 10511.
(35) Williams, D. H.; Fleming, I. *Spectroscopic Methods in Organic Chemistry*, 6th ed.; McGraw-Hill Higher Education: UK, 2008.
(36) Chen, C.; Chen, D.; Jiao, X.; Wang, C. *Chem. Commun.* **2006**, 4632.
(37) Chen, L.; Ma, X.; Liu, Y.; Zhang, Y.; Wang, W.; Liang, Y.; Zhang, Z. *Eur. J. Inorg. Chem.* **2007**, 4508.
(38) Labuschagne, P. W.; Kazarian, S. G.; Sadiku, R. E. *Spectrochim. Acta A* **2011**, *78*, 1500.
(39) Erbil, H. Y. *Surface Chemistry of Solid and Liquid Interfaces*; Blackwell Publishing Ltd: Oxford, UK, 2006.
(40) Ozin, G. A.; Arsenault, A. C. *Nanochemistry: A Chemical Approach to Nanomaterials*; The Royal Society of Chemistry, Cambridge, UK, 2005.
(41) Dloczik, L.; Konenkamp, R. *Nano Lett.* **2003**, *3*, 651.
(42) Newnham, R. E. *Properties of Materials: Anisotropy, Symmetry, Structure*; Oxford University Press: Oxford, UK, 2005.
(43) Zhu, H.; Yao, K.; Zhang, H.; Yang, D. *J. Phys. Chem. B* **2005**, *102*, 20676.
(44) Atkins, P.; Overton, T.; Rourke, J.; Weller, M.; Armstrong, F. *Inorganic Chemistry*, fourth ed.; Oxford University Press: Oxford, UK, 2006.
(45) Smyth, D. M. *The Defect Chemistry of Metal Oxides*; Oxford University Press: Oxford, UK, 2000.
(46) Zhou, L.; Wang, W.; Xu, H.; Sun, S.; Shang, M. *Chem.—Eur. J.* **2009**, *15*, 1776.
(47) Wu, J. M.; Zhang, T. W. *J. Photochem. Photobiol. A* **2004**, *162*, 171.
(48) Ashby, M.; Shercliff, H.; Cebon, D., Eds. *Materials engineering, science, processing and design*; Butterworth-Heinemann: Oxford, UK. 2007.
(49) Zhu, H.; Wang, X.; Qian, L.; Yang, F.; Yang, X. *J. Phys. Chem. C* **2008**, *112*, 4486.
(50) Bigioni, T. P.; Lin, X. M.; Nguyen, T. T.; Corwin, E.; Witten, T. A.; Jaeger, H. M. *Nat. Mater.* **2006**, *5*, 265.
(51) Liu, H. F.; Guo, B.; Hong, L.; Jiang, H. X. *J. Photochem. Photobiol. A* **2005**, *174*, 81.
(52) Chen, C.; Zhao, W.; Lei, P.; Zhao, J.; Serpone, N. *Chem.—Eur. J.* **2004**, *10*, 1956.
(53) Lachheb, H.; Puzenat, E.; Houas, A.; Ksibi, M.; Elaloui, E.; Guillard, C.; Herrmann, J.-M. *Appl. Catal., B* **2002**, *39*, 75.
(54) Sinha, A. K.; Basu, M.; Pradhan, M.; Sarkar, S.; Pal, T. *Chem.—Eur. J.* **2010**, *16*, 7865.
(55) Xu, H.; Zhang, L. *J. Phys. Chem. C* **2009**, *113*, 1785.
(56) Kemell, M.; Pore, V.; Tupala, J.; Ritala, M.; Leskelä, M. *Chem. Mater.* **2007**, *19*, 1816.